IOP Conf. Series: Journal of Physics: Conf. Series **810** (2017) 012012 doi:10.1088/1742-6596/810/1/012012

Self-absorption characteristics of measured laser-induced plasma line shapes

C G Parigger, D M Surmick and G Gautam

University of Tennessee Space Institute, Center for Laser Applications, 411 B.H. Goethert Parkway, Tullahoma, TN 37388, USA

E-mail: cparigge@tennessee.edu

Abstract. The determination of electron density and temperature is reported from line-of-sight measurements of laser-induced plasma. Experiments are conducted in standard ambient temperature and pressure air and in a cell containing ultra-high-pure hydrogen slightly above atmospheric pressure. Spectra of the hydrogen Balmer series lines can be measured in laboratory air due to residual moisture following optical breakdown generated with 13 to 14 nanosecond, pulsed Nd:YAG laser radiation. Comparisons with spectra obtained in hydrogen gas yields Abel-inverted line shape appearances that indicate occurrence of self-absorption. The electron density and temperature distributions along the line of sight show near-spherical rings, expanding at or near the speed of sound in the hydrogen gas experiments. The temperatures in the hydrogen studies are obtained using Balmer series alpha, beta, gamma profiles. Over and above the application of empirical formulae to derive the electron density from hydrogen alpha width and shift, and from hydrogen beta width and peak-separation, so-called escape factors and the use of a doubling mirror are discussed.

1. Introduction

The study of line shapes is essential for remote diagnosis of radiation emitted from a source. Plasma spectroscopy often relies on capturing emission characteristics for the purpose of determining physical parameters including assessments of dynamics [1, 2]. Equally, combustion physics addresses inferences from emitted atomic and molecular radiation. In this work, analysis of laser-induced plasma generated by focused, pulsed laser radiation is of interest, especially in view of self-absorption phenomena. A review is presented of general, expected appearances of emitted atomic line profiles that indicate re-absorption or self-absorption [3–8]. Standard techniques of Abel inversion are applied to gain information of the radiation source that appears very close to symmetric and optically thin for time delays of the order of 0.15 to 10 μs delay for ultra-high-pure (UHP) hydrogen gas and 0.4 to 10 μs for standard ambient temperature and pressure (SATP) laboratory air. In the context of the treatment of self-absorption and line-reversal, the escape factor approach is discussed [9–11]. The experiments also utilize a so-called doubling mirror for the evaluation of the degree of self-absorption [12, 13]. The measurements primarily concentrate on the hydrogen Balmer series lines with some references to the recorded ionized nitrogen lines in the SATP moisture-containing laboratory air [14, 15]. The experimental arrangement includes the use of Q-switched, 1064-nm Nd:YAG laser radiation of 13 to 14 ns duration with pulse energies of 170 mJ. Laser-induced plasma is generated by focusing the laser beam from the top, aligned parallel to the the slit of a Czerny-Turner spectrometer equipped with a 1200 grooves/mm holographic grating and an intensified charge coupled detector (ICCD) to record temporally and spatially resolved spectra with a 10-ns gate-width that are wavelength and sensitivity

corrected. Further details regarding the focusing and collection optics, laser device, cell for the UHP hydrogen and SATP air experiments are reported elsewhere including video of typical procedures [16].

2. Escape factor and self-absorption

The escape factor describes the amount of radiation that emanates from a radiation source, and it can be utilized to determine the amount of self-absorption. Three separate integrations are usually required to evaluate this factor [12]. First, an integration over the frequency interval of the emitting line profile while assuming complete redistribution of radiation, second, a surface integral to find the amount of radiation that escapes, and third, a volume integral over the extent of the source. For a point-like source that is usually described by a Dirac delta distribution, both surface and volume integrals are easily evaluated leading to the expected transmission factor, $T(\tau_0)$, as function of the optical thickness, τ_0,

$$T(\tau_0) = \int L(\nu) \exp\{-\tau_0 L(\nu)/L_0\} d\nu, \tag{1}$$

with the line profile, $L(\nu)$, normalized by the maximum, L_0, at line center. The optical thickness is related to the opacity, K_0, and absorption length, ℓ, as usual, $\tau_0 = K_0\ell$. For the line profile of the laser-induced plasma source, a Lorentzian and a double-peaked profile are typically used to describe the central regions of Stark-broadened hydrogen Balmer alpha and beta lines, respectively [17–19]. For a delta-distributed line profile [12], Equation (1) yields the expected result for a transmission factor of $\exp\{-\tau_0\}$. Figure 1 illustrates the integrand of the transmission factor for increasing values of τ_0.

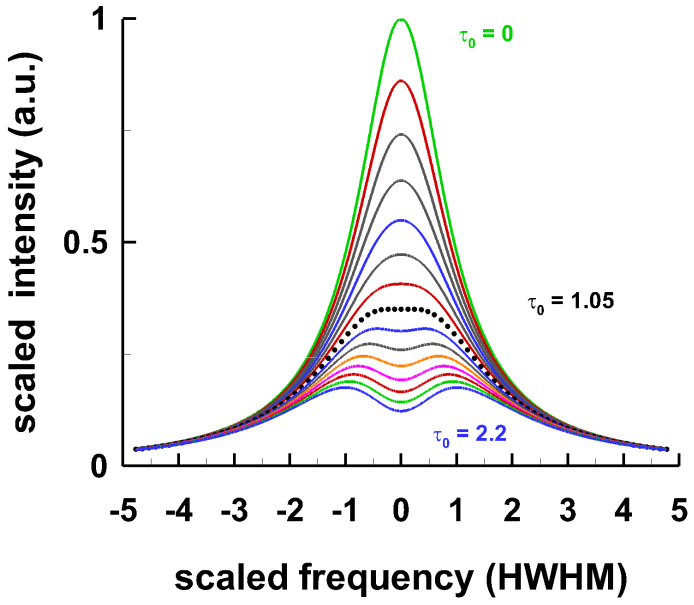

Figure 1. Integrand of the transmission factor for optical thickness values of $\tau_0 = 0$ to 2.20 for a Lorentzian vs. frequency, scaled with respect to the half-width-at-half-maximum (HWHM). For $\tau_0 = 1.05$, the central region shows a reduction by a factor of three from the optical thin line limit $\tau_0 \to 0$ and an increase of the HWHM by a factor of 2. For $\tau_0 = 2.20$, line reversal is clearly developed.

Computations of the escape factors for constant, spherically symmetric distributions of radiators [10] show diminished self-absorption effects and absence of line-reversal in the 0 to 2.20 range for the optical thickness, τ_0.

3. Doubling mirror method

Assessment of the level of self-absorption can be accomplished by including a so-called signal doubling mirror in the experimental arrangement [12]. In a practical realization, also a second lens is utilized for the purpose of matching the radiation source volume that is imaged onto

the slit of a spectrometer [13]. The signal should be doubled for an ideal lens and mirror. Consideration of optically thin conditions, i.e., for $\tau_0 \to 0$ or when $\exp\{-\tau_0\} \approx 1-\tau_0+\tau_0^2/2$, leads to the correction factor, $K_{\lambda,\mathrm{corr}}$, that can be applied to measured line-of-sight spectra to adjust for self-absorption. The self-absorption corrections are based on the ratios of the wavelength dependent signals, R_λ, and the continuum contribution, R_C,

$$K_{\lambda,\mathrm{corr}} = \frac{\ln\{y_\lambda\}}{y_\lambda - 1} \qquad \text{with} \qquad \mathrm{y}_\lambda = \frac{\mathrm{R}_\lambda - 1}{\mathrm{R_C} - 1}. \tag{2}$$

The ratios R_λ and R_C are found by comparing recorded data with and without the doubling mirror. As the correction factors are applied, not only values for the spectral peaks but rather the entire profile is corrected for distortions including slight shifts of the line's center wavelength. The inverse of the average of the correction factor, $1/\langle K_{\lambda,\mathrm{corr}}\rangle$, corresponds to the self-absorption factor, SA.

A method for determination of self-absorption due to free-free or inverse Bremsstrahlung would be direct measurement of the optical thickness from the plasma emission coefficient and the plasma radius [20]. The value of the self-absorption, SA, at line center is evaluated using

$$SA = \frac{1-\exp\{-\tau_0\}}{\tau_0} \qquad \text{and} \qquad \mathrm{SA} \approx 1-\tau_0/2 \qquad \text{for} \qquad \tau_0 \ll 1. \tag{3}$$

The determination of the value of the average self-absorption using this method, however, in absence of spectral lines and with the continuum radiation dominating the emission spectrum, would require tedious absolute calibration of the detector. In comparison, the doubling mirror method yields wavelength-dependent factors for correction of the self-absorption distortions.

4. Abel inversion of line-of-sight data

Spatial information about the radiation source can be extracted from laterally recorded data. The initially expanding laser induced plasma reveals asymmetries associated with focusing and induced including plasma dynamics. However, from recorded shawdowgraphs of the plasma dynamics, largely spherically symmetric expansion appears to occur for time delays of 0.1 to to 10 µs after initiation of optical breakdown. Given a close to symmetric plasma kernel, standard Abel inversion techniques are applied in the study of the expanding plasma [21].

In the experiments, lateral spectral data are recorded with an intensified charge coupled device (ICCD), the horizontal data corresponds to spectral information, the vertical data correspond to the lateral spatial information. For time delays of 0.15 and 0.40 µs for the UHP hydrogen gas in a cell, and for the time delay of 0.40 µs in SATP air, Abel inversion is performed using an adapted Abel-inversion method [22].

In a variety of laser-induced breakdown spectrosocpy (LIBS) arrangements, an optical fiber is utilized to couple the plasma radiation to a multi-order echelle-type spectrograph for highly resolved spectra across a substantial coverage from typically 200 to 900 nm. However, when employing an ICCD with a reasonable two-dimensional coverage of 1024×1024 pixels, a narrower spectral range is measured horizontally but with spatial resolution along the vertical axis. Stark-broadened hydrogen profiles are adequately covered, e.g., over a 24 nm wavelength range for the hydrogen beta, H_β, line when using a 1200 grooves/mm grating in a 0.64 m Czerny-Turner type spectrometer. The spatial resolution along the vertical direction amounts to about 13.8 mm that is sufficient to capture the expanding plasma when using 1:1 imaging.

The line-of-sight measurements portray a sum of contributions along the radiation source,

$$I(z,\lambda) = 2\int_z^R I(r,\lambda)\frac{r}{\sqrt{r^2-z^2}}dr. \tag{4}$$

Here, $I(z,\lambda)$ and $I(r,\lambda)$ denote the measured lateral spectra (along the slit height, z) and radial wavelength-dependent intensity distributions, respectively. The dependence on wavelength, λ, of the measured and radial distributions is explicitly included due to the use of the dispersive, holographic grating. The upper integration limit, R, is usually much larger than the object dimension, δ, or in other words $R \gg \delta$. The factor of 2 indicates top/bottom symmetry.

In this work, the Abel inverse transform is computed without the need for pre-treating the recorded data [22, 23], leading to inverted intensity values, $I(r,\lambda)$, with errors of only a few percent for selected test cases. Moreover, the strict requirement for axial symmetry, specifically spherical symmetry, can be slightly relaxed following procedures that were utilized originally in the analysis of inductively coupled plasma sources but have been adapted to the analysis of expanding laser-induced plasma [24].

In the analysis of the UHP hydrogen experiments recorded for the time delays of 0.15 and 0.40 μs, the spectra for hydrogen alpha, beta and gamma lines are each Abel inverted, and subsequently fitted to known line profiles. For H_α and H_γ Lorentzians are used to extract background, shift and full-widths-at-half-maximum, and for H_β asymmetric line profiles are directly fitted to find the electron density, N_e. Boltzmann plots are generated to evaluate the electron excitation temperature. The SATP laboratory data at a time delay of 0.4 μs show the hydrogen alpha, H_α, line together with two ionized nitrogen lines, the H_β line is not visible due to the relatively large free electron background contribution caused by the presence of mainly nitrogen and oxygen. The electron densities are evaluated from H_α widths and shifts using recently communicated formulae [18].

5. Electron density results

The electron density in the range of 0.5 to 50×10^{17} cm^{-3} is evaluated from the hydrogen alpha, H_α, Balmer series line. For electron densities of 0.5 to 5×10^{17} cm^{-3}, the hydrogen beta, H_β, line is preferred. Due to the asymmetric appearance, direct fitting is accomplished using predicted H_β line profiles including comparisons with results from width and peak-separation predictions [25–30].

The recorded H_α spectra are fit to Lorentzians to extract the FWHM, Δw_{H_α}, and red-shifts, $\Delta\delta_{H_\alpha}$, and then the empirical formulae [18],

$$\Delta w_{H_\alpha}[nm] = 1.31\left(\frac{\mathrm{N_e[cm^{-3}]}}{10^{17}}\right)^{0.64\ \pm\ 0.03}, \tag{5}$$

$$\Delta\delta_{H_\alpha}[nm] = 0.055\left(\frac{\mathrm{N_e[cm^{-3}]}}{10^{17}}\right)^{0.97\ \pm\ 0.03}, \tag{6}$$

yield measures for the electron densities. The red shift shows an almost linear dependence on electron density but would show relatively large error bars for electron densities of the order of 1×10^{17} cm^{-3} due to the spectral resolution of $\delta_R = 0.1$ nm. The width however yields results with an error of the order of 25%. Fitting with Lorentzians is quite acceptable considering the minute effect of Gaussian instrument broadening that would in principle result in Voigt profiles.

The H_β empirical formulae can be applied as well for electron densities up to $\simeq 5\times10^{17}$ cm^{-3} for pure hydrogen optical breakdown experiments [18],

$$\Delta w_{H_\beta}[nm] = 4.50\left(\frac{\mathrm{N_e[cm^{-3}]}}{10^{17}}\right)^{0.71\ \pm\ 0.03}, \tag{7}$$

$$\Delta\lambda_{ps}[nm] = 1.32\left(\frac{\mathrm{N_e[cm^{-3}]}}{10^{17}}\right)^{0.61\ \pm\ 0.03}. \tag{8}$$

The peak separation, $\Delta\lambda_{ps}$, has been investigated in view of assessing self-absorption effects. For electron densities of $\simeq 1{\times}10^{17}$ cm^{-3}, the H_β peak separations yield results consistent with the ones obtained from the widths. Measurements of the widths are preferred to determine electron densities of the order of $\simeq 5{\times}10^{17}$ cm^{-3} rather than finding the values for the peak separation [29, 30].

5.1. Air plasma results

Application of the Abel inversion and reconstruction of the spectra along the line of sight yield spatially resolved electron densities along the line of sight. Figure 2 and 3 display the recorded line profile corresponding to the edge of the plasma and the radial variation, respectively.

Figure 2 also shows the Savitzky-Golay filtered data and the results of fitting the data including provision for the self-absorption but excluding the regions for the singly ionized nitrogen lines. For a density of $N_e = 20{\times}10^{17}$ cm^{-3}, self-absorption effects are illustrated in Fig. 2 by the apparent line reversal in the dip near line center of the fitted Lorentzians. The H_α line shape reveals distortions with contributions to line-widths primarily due to Stark broadening. Evidence of self-absorption is also confirmed by the indicated red shift and by comparison of the electron densities with results obtained from the N^+ lines [14]. Figures 4 and 5 illustrate a 3-dimensional cross-sections of N_e obtained from fitting widths and shifts, respectively.

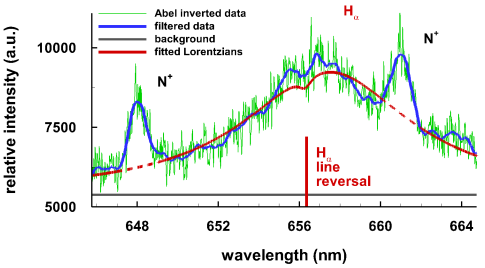

Figure 2. SATP air, $N_e = 20{\times}10^{17}$ cm^{-3}, $\tau = 0.40$ µs,

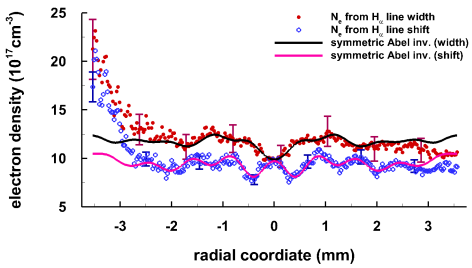

Figure 3. N_e variation from fitting Abel-inverted spectra.

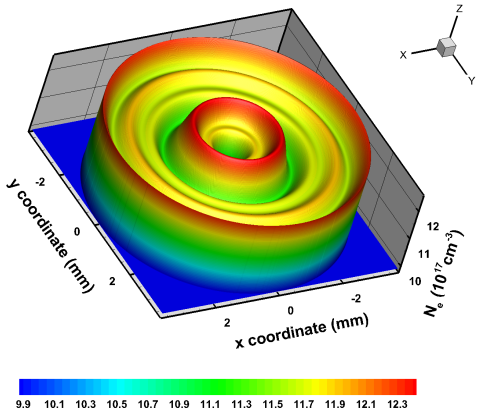

Figure 4. N_e obtained from H_α widths.

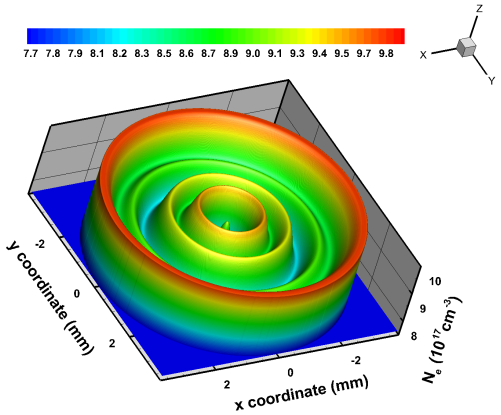

Figure 5. N_e obtained from H_α shifts.

Standard and extended, asymmetric Abel transforms reveal almost identical results in the central 5 mm range. This confirms the hypothesis of spherically symmetric expansion suggested from shadowgraphs.

For a time delay of 0.4 μs, self-absorption effects have been reported based on the doubling mirror method for recorded line-of-sight H_α data [13]. Considering the corrections and the usual, absolute error bars associated with electron density determinations from the hydrogen alpha line, the self-absorption effects caused changes of the electron density within the error bars.

5.2. Hydrogen plasma results

In this section, electron density results are presented of laser-induced plasma in ultra-high-purity (UHP) hydrogen gas contained in a cell. Figure 6 portrays Abel inverted spectra, Savitzky-Golay filtered results, and the fitted Lorentzian. The line reversal manifests self-absorption.

Comparisons of the electron densities inferred from H_α and H_β are expected to yield results within the associated error bars. Figure 7 indicates larger values for N_e obtained from the H_α line near the plasma edge indicating self-absorption. In the 2 mm central region, the electron density results appear to be within the error bars except for the very center. Also, the central region indicates close to spherical symmetric plasma. For a later time delay of 0.4 μs, analysis of the hydrogen beta data shows almost spherically symmetric results for the electron density within the 2 mm central core.

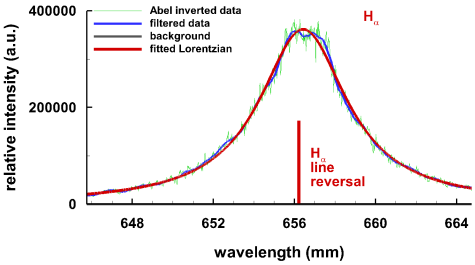

Figure 6. $N_e = 8.4\times10^{17}$ cm^{-3}, UHP hydrogen gas (810 Torr), $\tau = 0.15$ μs.

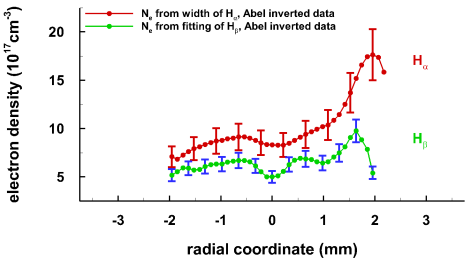

Figure 7. N_e from fitting Abel-inverted H_α and H_β line profiles.

For the recorded data at the time delay of $\tau = 0.40$ μs, Boltzmann plots are constructed from the H_α, H_β and H_γ lines. Integrated line shapes are utilized to provide a measure for the temperature distribution. Figure 8 reveals a cooler central region and a relatively hot ring of the order of 100,000 K (8.6 eV) and . Noteworthy, the kernel expands at or near the speed of sound in hydrogen gas. From Fig. 8, the two temperature peaks near ± 0.5 mm at a time delay of 0.4 μs would indicate an expansion speed of 1.25 km/s. The average temperature along the line of site is consistent with previous experimental investigations. Fig. 9 shows corresponding electron densities. The error bars are in part due to the lower fidelity in the Abel inversion for a time delay of 0.40 μs.

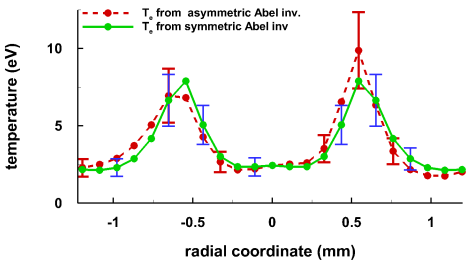

Figure 8. T_e determined from Boltzmann plots, $\tau = 0.40$ μs.

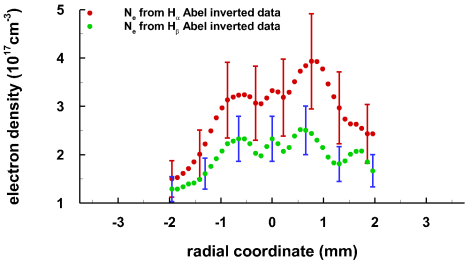

Figure 9. N_e is almost symmetric in the -1 to +1 mm range, $\tau = 0.40$ μs.

6. Conclusions

Analyses of the laser-induced plasma using standard Abel transforms reveal that the central core is close to spherically symmetric at time delays of 0.15 and 0.40 μs for UHP hydrogen gas, and at 0.40 μs for SATP laboratory air. Abel inverted spectra confirm occurrence of self-absorption. The self-absorption phenomena cause line shape distortions and line-reversals. These appear to be insignificant in the electron density determination for $N_e \leq 20\times10^{17}$ cm^{-3} in the presented time-resolved experimental results of laser-induced plasma in UHP hydrogen gas and SATP laboratory air. The temperature distributions in the hydrogen plasma experiments reveal as well a ring structure indicating lower T_e in the central core region, and this central region expands at or near the speed of sound in hydrogen gas.

Acknowledgments

The authors acknowledge A. M. and Th. M. EL Sherbini for their continued interest in this work, and thank for support in part by the Center of Excellence, Center for Laser Applications (CLA) and the University of Tennessee Space Institute.

References

[1] Kunze H-J 2009 *Introduction to Plasma Spectroscopy* (Springer-Verlag, Berlin)
[2] Mulser P and Bauer, D 2010 *High Power Laser-Matter Interaction* (Springer-Verlag, Berlin)
[3] Holstein T 1947 *Phys. Rev.* **72** 1212
[4] Holstein T 1951 *Phys. Rev.* **83** 1159
[5] Cowan R D and Dieke G H 1948 *Rev. Mod. Phys.* **20** 418
[6] Pardini L, Legnaioli S, Lorenzetti G, Palleschi V, Gaudiuso R, De Giacomo A, Diaz Pace D M, Anabitarte Garcia F, de Holanda Cavalcanti G and Parigger C 2013 *Spectrochim. Acta Part B* **88** 98
[7] Aragón C and Aguilera J A 2010 *Spectrochim. Acta Part B* **65** 395
[8] Kielkopf J F and Allard N F 2014 *J. Phys B: At. Mol. Opt. Phys.* **47** 155701
[9] Irons F E 1979 *J. Quant.Spectrosc. Radiat. Transfer* **22** 1
[10] Mancini R C, Joyce R F and Hooper Jr C F 1987 *Phys B: At. Mol. Opt. Phys.* **20** 2975
[11] Fill E E 1988 *J. Quant.Spectrosc. Radiat. Transfer* **39** 489
[12] Moon H-Y, Herrera K K, Omenetto N, Smith B W and Winefordner J D 2009 *Spectrochim. Acta Part B* **64** 702
[13] Parigger C G, Gautam G, Woods A C, Surmick D M and Hornkohl J O 2014 *Trends Appl. Spectrosc.* **11** 1
[14] Parigger C G, Swafford L D, Surmick D M, Witte M J, Woods A C and Gautam G 2014 *J. Phys.: Conf. Ser.* **548** 012043
[15] Swafford L D, Surmick D M, Witte M J, Woods A C, Gautam G and Parigger C G 2014 *J. Phys.: Conf. Ser.* **548** 012049
[16] Parigger C G, Woods A C, Witte M J, Swafford L D and Surmick D M 2014 *J. Vis. Exp.* **84** e51250
[17] Gautam G and Parigger C G 2014 *Int. Rev. At. Mol. Phys.* **5** 115
[18] Surmick D M and Parigger C G 2014 *Int. Rev. At. Mol. Phys.* **5** 73
[19] EL Sherbini A M, Surmick D M, Gautam G and Parigger C G 2014 *Int. Rev. At. Mol. Phys.* **5** 23
[20] Parigger C G, Surmick D M, Gautam G and EL Sherbini A M 2015 *Opt. Lett.* **40** 3436
[21] Parigger C G, Surmick D M and Gautam G 2015 *Int. Rev. At. Mol. Phys.* **6** 41
[22] Pretzler G 1991 *Z. Naturforsch.* **46a** 639
[23] Killer C 2014 http://www.mathworks.com/matlabcentral/fileexchange/43639-abel-inversion-algorithm [last accessed Nov 15 2015]
[24] Blades M W 1983 *Appl. Spectrosc.* **37** 371
[25] Djurović S, Ćirišan M, Demura A V, Demchenko G V, Nikolić D, Gigosos M A and Gonzáles M Á 2009 *Phys. Rev. E.* **79** 046402
[26] Palomares J M, Torres J, Gigosos M A, van der Mullen J J A M, Gamero A and Sola A 2009 *Appl. Spectrosc.* **63** 1023
[27] Palomares J M, Torres J, Gigosos M A, van der Mullen J J A M, Gamero A and Sola A 2010 *J.Phys.: Conf. Ser.* **207** 012013
[28] Ivković M, Konjević N and Pavlović Z 2015 *J. Quant. Spect. Radiat. Transfer* **154** 1
[29] Gautam G, Surmick D M and Parigger C G 2015 *J. Quant. Spect. Radiat. Transfer* **160** 19
[30] Gautam G, Parigger C G, Surmick D M and EL Sherbini A M 2016 *J. Quant. Spect. Radiat. Transfer* **170** 189